Chinese Chemical Letters 32 (2021) 983–989

Contents lists available at ScienceDirect

Chinese Chemical Letters

journal homepage: www.elsevier.com/locate/cclet

Review

Na-K liquid alloy: A review on wettability enhancement and ionic carrier selection mechanism

Xinran Li[a,1], Jiahao Liu[a,1], Cheng Chen[a], Jian Yang[a], Ziqiang Xu[a,*], Mengqiang Wu[a,*], Yuesheng Wang[b,*], Zaghib Karim[b]

[a] School of Materials and Energy, University of Electronic Science and Technology of China, Chengdu 611731, China
[b] Center of Excellence in Transportation Electrification and Energy Storage, Hydro-Québec, Varennes, QC J3X1S1, Canada

ARTICLE INFO

Article history:
Received 4 June 2020
Received in revised form 3 August 2020
Accepted 14 September 2020
Available online 15 September 2020

Keywords:
Liquid electrode
Na-K alloy
Dendrite inhibition
Wettability improvement
Carrier selectivity

ABSTRACT

The intrinsic liquid interface of Na-K alloy allays concerns about dendrite growth on metal anodes that are thermodynamically within the room temperature (20–22 °C). Nevertheless, it hinders the formation of a stable electrode structure due to the inferior wettability induced by considerable liquid tension. In addition, the dominant ionic carrier in the Na-K alloy is subject to multiple factors, which is not conducive to customized battery design. This review, based on recently reported frontier achievements on Na-K liquid anodes, summarizes practical strategies for promoting the wettability by high-temperature induction, capillary effect, vacuum infiltration, and solid interface protection. Furthermore, four selection mechanisms of the dominant ionic carrier are presented: (1) ion property dominated, (2) cathode dominated, (3) separator dominated, and (4) solid electrolyte interface dominated. Notably, initial electrolytes in energy storage systems have been unable to play a decisive role in ionic selection. Utilizing a superior wettability strategy and simultaneously identifying the dominant ionic carrier can facilitate the tailored application of dendrite-free Na-K liquid anodes.

1. Introduction of Na-K alloy

Solid alkali metal anodes have higher energy densities than those of corresponding alkali ion batteries. However, the intrinsic dendritic growth on metal anodes leads to battery failure and thermal runaway. From a thermodynamics perspective, the mechanisms leading to dendritic growth can be classified into four theoretical models: the surface energy and ionic migration energy model, the heterogeneous nucleation model [1,2], the Chazalviel space charge model [3,4] and the solid electrolyte interphase (SEI)-induced nucleation model. Based on the mechanisms mentioned above, several efforts have led to practical strategies, which include electrolyte optimization [5–7], depositing artificial SEI [8–10], preparing three-dimensional electrodes, guiding non-vertical dendritic growth [11], introducing artificial nucleation sites [10] and employing solid electrolytes [12,13]. Nevertheless, the abovementioned strategies are unable to provide a homogeneous surface-barrier distribution during cycling, leading to dendritic growth.

It is reported that adopting liquid anodes can form a uniform barrier interface, eliminating nucleation sites for dendritic growth [14–16], such as Li-Sb-Pb alloy anodes, Mg-Sb alloy anodes [14,17–20] and other molten electrodes [21]. Unfortunately, molten anodes generally have high melting points or eutectic temperatures [14] higher than 300 °C, which may result in metal erosion [22] and pose a safety risk. Therefore, developing a room-temperature liquid anode is of great interest.

Sodium-based alkali metal alloys can be liquefied across a wide proportional range at room temperature; such alloys include Na-K, Na-Rb, Na-Cs [15]. The high chemical activities of Rb and Cs have hindered their application in energy storage. However, several studies have confirmed the practicability of Na anodes [23] and K anodes [24] for relatively mild activity. As demonstrated in the phase diagram of the Na-K alloy, the proportion of Na should be 9.2–58.2 wt% at room temperature to maintain a dendrite-free liquid state [25,26]. Na-K liquid alloys are equipped with various electrochemical advantages, such as high electronic conductivity, self-repair ability, and high energy density [27–29]. From recent

* Corresponding authors.
E-mail addresses: nanterxu@uestc.edu.cn (Z. Xu), mwu@uestc.edu.cn (M. Wu), Wang.Yuesheng@ireq.ca (Y. Wang).
[1] These authors contributed equally to this work.

https://doi.org/10.1016/j.cclet.2020.09.018
1001-8417/

reports, Na-K liquid alloys have been applied to K metal batteries [30–33], K ion capacitors [34–36], K-O_2 batteries [37], flow batteries [38] and other systems.

Among the reported works on Na-K alloy anodes, three types of symmetric batteries of Na-K, pure Na, and pure K systems have been employed to study dendritic growth indirectly by comparing the voltage polarization after prolonged charging and discharging. Zhang [30] observed the fluctuation of voltage [39–41], revealing that a Na-K symmetric battery remained stable over 1800 h, whereas a Na symmetric battery had obvious voltage fluctuation, indicating the formation and fracture of dendrites. Nonetheless, fluctuations are still observed for Na-K symmetric batteries during the first few cycles. Goodenough [22] attributed the slight fluctuations of the first ten cycles to the establishment of a liquid–liquid interface [42]. In his experiment, the Na symmetric battery exploded after 465 h, whereas the Na-K battery lasted longer. Compared with a K symmetric battery, Tu [13] also found that a Na-K@C symmetric battery showed longer-lasting voltage stability in the case of long-term operation.

Granted that Na-K liquid alloys exhibit notably practical potentiality in terms of dendrite inhibition, what prevents its further development is its poor wettability and whether the dominant ionic carrier is Na^+ or K^+:

(1) Poor wettability is an intrinsic defect of Na-K alloys due to their strong surface tension [22,31,34,43]. Hence, they are unable to develop a stable morphologic structure that enables contact with the current collector, commercial separator, or solid electrolyte [15,22].

(2) The dominant ionic carrier (Na^+ or K^+) in the charging and discharging of Na-K liquid anode battery remains to be determined. Once determined, a tailored battery system can be realized by selecting the appropriate electrolyte, separator, and cathode, ultimately enhancing battery performance.

This article summarizes recent research on liquid Na-K alloys, promoting a theoretical understanding and application of such alloys to improve the wettability of Na-K alloys and to understand the selection mechanism of the dominant ionic carrier. The tendency of application and prospects is put forward in the end.

2. Wettability enhancement

The strategies for wettability are classified into four types as drawn in Figs. 1a-d: (1) employing vacuum infiltration [31,32,44] to promote absorption of the Na-K alloy; (2) increasing the specific surface area and porosity of the substrate, which introduces a capillary effect [30,34]; (3) introducing an in-situ self-assembly interface layer to develop a stable morphologic structure [13]; (4) or raising the contact temperature between the substrate and the Na-K alloy [22].

Goodenough [22] adopted carbon paper to absorb the Na-K (K: 66.3 wt%) alloy inspired by silicone materials [45,46], and he observed a subtle wetting effect at room temperature. Only when the contact temperature between two materials increased to 420 °C was the liquid Na-K alloy absorbed by the carbon paper at a relatively fast rate. At this temperature, the carbon paper presented good loading, such that its absorption of the Na-K alloy was 1:5 (mass ratio). Both the carbon paper and the Na-K alloy could be recycled and separated by using tetraethylene glycol dimethyl ether (TEGDME). From the point of spreading coefficient, specific surface free enthalpy decreases with increasing temperature, signifying the reduction of surface tension. According to the Young's theory, with the decrease of gas-liquid surface tension, the contact angle will go down. Hence high temperature resulted in a small contact angle with excellent fluidity, leading to enhanced wettability of Na-K alloy. However, a high-temperature operation will accelerate the occurrence of metal erosion and various side effects, resulting in additional thermal management costs.

The capillary effect of the anode substrate was applied in the lasting absorption of a Na-K alloy at room temperature. In Zhang's research [30], the oxygen doping of carbon cloth was realized by utilizing $KMnO_4$ after soaking the cloth with a mixed acid (H_2SO_4: HNO_3 = 1:3). Finally, a porous nanocarbon cloth with oxygen groups (oxygen content was 12.7%) was obtained by air heat treatment at 400 °C. Benefiting from the abundant oxygen groups, the surface area of the treated carbon cloth increased from 0.7061 m^2/g to 3.2784 m^2/g, and the carbon cloth with numerous defects revealed strong affinity [47] and good wettability. Consequently, the contact angle between the carbon cloth and the Na-K alloy decreased from 146° to 0°. Also based on the capillary effect, Yang [34] reported a super directionally arranged carbon nanotube membrane (CM). It was textured by super-oriented carbon nanotubes (CNTs) with tiny O_2 structures whose presence was confirmed by X-ray photoelectron spectroscopy (XPS) [48]. This arrangement showed excellent absorption of the Na-K alloy with good flexibility. Furthermore, the contact angle between the Na-K alloy and CM was always less than 90°. The color of the absorbed Na-K alloy surface changed from dull black to bright silver, which proved the corresponding result.

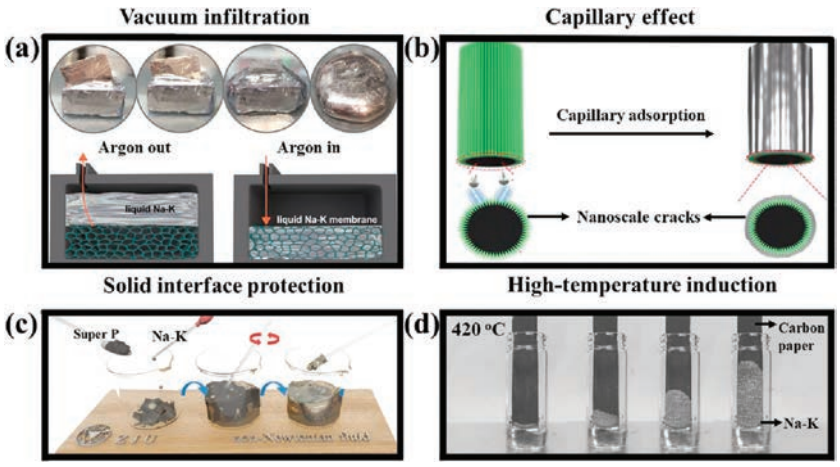

Fig. 1. Four strategies for Na-K alloy wettability. (a) Vacuum infiltration. Reproduced with permission [31]. Copyright 2018, Wiley. (b) Capillary effect. Reproduced with permission [30]. Copyright 2020, Electrochemical Society, Inc. (c) Solid interface protection. Reproduced with permission [13] Copyright 2018, Wiley. (d) High-temperature induction. Reproduced with permission [22]. Copyright 2016, Wiley.

Vacuum infiltration has also been used to enhance the wettability. Yu [32] and Xue [31] both achieved high loading of Na-K alloys into carbon cloth substrates at room temperature by vacuum infiltration. Specifically, in an argon glove box, a carbon cloth was soaked in a Na-K solution before being transferred to a vacuum chamber to extract and infiltrate argon. The argon in the substrate was extracted first under pressure; after that, the pores of the substrate were rapidly immersed in a liquid Na-K alloy in a subsequent inflation process. The vacuum infiltration treatment resulted in an anode structure with a distinct metallic luster, implying that the Na-K alloy was distributed evenly into the substrate. This strategy also can be expanded using various systems of foamy copper, foamy nickel, and other porous structures.

The wettability of a Na-K alloy can also be improved using a solid interface structure. Tu [13] devised an *in-situ* solid interface structure for the first time, realized a coating of Na-K alloy (K: 78 wt%) and formed a liquid–solid–liquid interface of a Na-K alloy ||*in-situ* interface|| electrolyte. This *in-situ* interface was composed of a compact and thin solid K_2O layer. When Na contacted the K, liquid metal formed on the junction point and rapidly diffused to other parts, finally forming a liquid alloy. Theoretically, this junction reaction is exothermic, and the heat it releases will accelerate the reaction between trace amounts of O_2 in the glovebox and K metal to form K_2O for high chemical activity of K. Subsequently, the K_2O will cover the K-Na alloy and form a solid–liquid interface (K_2O@Na-K). In the validating experiment, the Na-K alloy extracted directly from the K_2O@Na-K could not form K_2O in the glovebox because of inadequate heat. Interestingly, as for other K oxides such as KO_2 and K_2O_2, they will transform to K_2O ultimately after thermal activation [49,50], as shown in Eqs. (1) and (2). The contact angle between K_2O@Na-K and the carbon fiber cloth (CFC) was 50°, much less than the initial 150° of the Na-K alloys. The K_2O layer not only improved the wettability but also possessed a self-healing ability. Attributed to the tension of Na-K and the binding force of K_2O itself, the outer K_2O restored itself rapidly within 2 s after mechanical damage and reformed a liquid–solid–liquid interface0.

$$2KO_2(s) + 2K(l) = 2K_2O(s) + O_2(g)\ \Delta_r G^0_{298} = -164\ \text{kJ/mol}$$

$$K_2O_2(s) + 2K(l) = 2K_2O(s)\ \Delta_r G^0_{298} = -217\ \text{kJ/mol}$$

The abovementioned strategies, *i.e.*, high-temperature induction, capillary effect, and vacuum infiltration, do not obviously modify the tension of Na-K alloys intrinsically; therefore, the Na-K alloy immersed in a substrate would be squeezed out again under external stress. Consequently, Tu [33] eliminated the intrinsic tension of Na-K alloys through a non-Newtonian interface technology by virtue of a non-Newtonian fluid. Tu stirred Na-K alloy (K: 22 wt%) and Super P powder manually at room temperature and obtained a stable non-Newtonian Na-K@C solid–liquid interface (0.1 mL KNa and 16.7 mg Super P); the particle size was 300 nm. The reaction between trace amounts of H_2O, O_2 and K to form K_2O and KOH (< 0.0431 wt%) provided the binding force for Super P and the Na-K alloy. It also played a huge role in increasing the viscosity of the Na-K alloy and reducing the surface tension. As a result, the contact angle formed between the copper foil collector and Na-K@C with certain self-healing properties was approximately 0°.

To summarize, defect engineering to introduce the capillary effect on the substrate surface can provide storage spaces for Na-K with the help of vacuum infiltration and high-temperature induction, and thus enhance the wettability of Na-K to realize rapid injection. In addition, by employing a solid interface, good wettability can be achieved intrinsically, thereby promoting the bonding performance between the Na-K alloy and the substrate.

In addition to the abovementioned four wettability methods based on the Na-K alloy itself, structural perspectives from current collector and electrolyte interface also occupy prospective crucial positions to form a stable Na-K anode. To establish a stable and affiliative electrolyte-anode interface, Yu [51] employed the time-

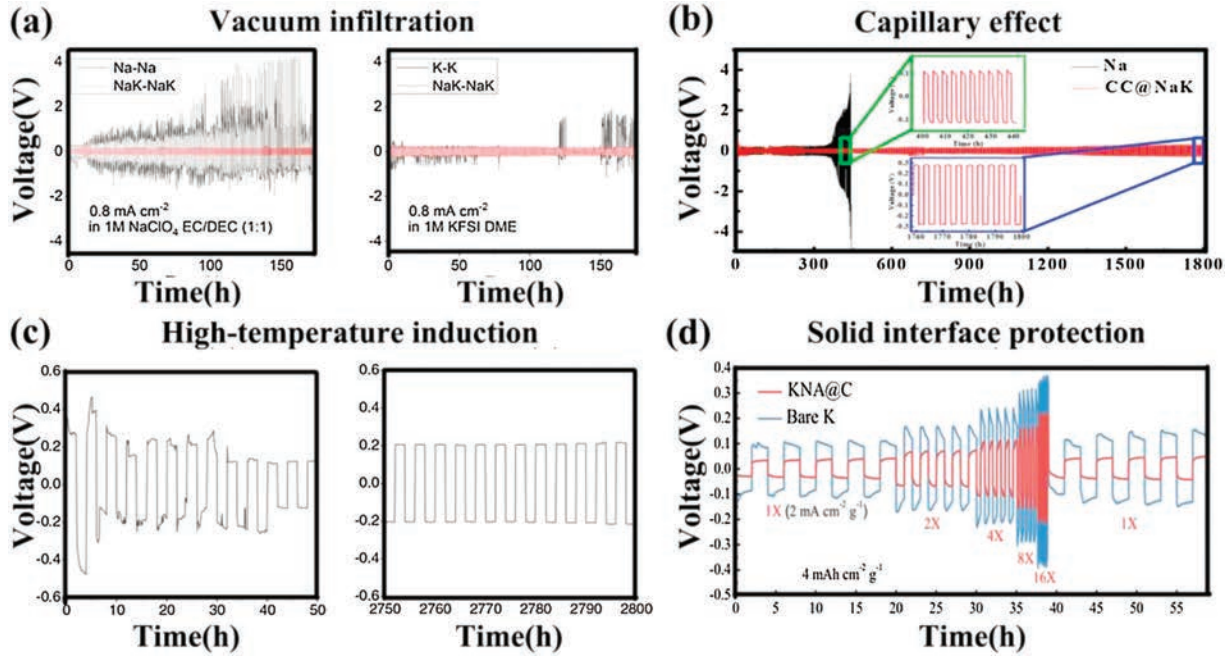

Fig. 2. Voltage profiles after different wettability treatment. (a) Na-Na, K-K and NaK-NaK symmetric batteries. Reproduced with permission [31]. Copyright 2018, Wiley. (b) Na-Na and NaK-NaK with capillary carbon. Reproduced with permission [30]. Copyright 2020, Electrochemical Society, Inc. (c) High-temperature induction. Reproduced with permission [22]. Copyright 2016, Wiley. (d) Solid interface protection. Reproduced with permission [13]. Copyright 2018, Wiley.

of-flight secondary-ion mass spectrometry (TOF-SIMS) to demonstrate the organic electrolyte with fluoroethylene carbonate (FEC) is able to shape the stable solid interface on Na-K alloy. Similarly, Kang [52] employed the cross-linked beta alumina nanowires coated by a poly-based gel polymer electrolyte to construct an inorganic ionic conductor/gel polymer electrolyte composite, resulting in the formation of a uniform SEI which led to an enhanced adhesive force between electrolyte and Na-K alloy. Furthermore, the existence of solid-liquid hybrid Na-ion transportation channels in hybrid electrolytes was proposed, indicating that the transportation channels of Na-ion and K-ion in Na-K alloy battery with superior ionic conductivity and cycle performance were identical. David Mitlin [53] designed a 3D compound substrate to adjust the surface tension of current collector from chemical and geometrical effects. This strategy was also implemented on carbonaceous substrate in Na-O2 batteries [54].

3. Electrochemical analysis for Na-K system

Symmetric and asymmetric battery systems were employed in related literatures without exception to characterize the electrochemical properties of Na-K alloy anode with different concerns.

For symmetric system, all the four strategies induced Na-K symmetric batteries present similar voltage profiles with dendrite inhibition features during the plating/stripping process. Compared with Na-Na and K-K symmetric systems, NaK-NaK symmetric batteries possess several impressive electrochemical characteristics: (1) NaK-NaK proves to have the thinnest hysteresis voltage as shown in Figs. 2a-d, indicating a relatively ideal metal deposition without obvious metal dendrite; (2) According to Figs. 2a and b, bare Na/K symmetric batteries inevitably show improving voltage hysteresis as time goes on. However, the Na-K one is able to hold no significant change, *i.e.*, it can sustain prolonged uniform plating/stripping; (3) Fig. 2d displays the self-recovery feature of Na-K that the voltage hysteresis can return to the initial value after undergoing a huge current density of 32 mA cm^{-2} g^{-1}; (4) However, Fig. 2c confirms that voltage fluctuation of Na-K anode will also happen in first few cycles for interface establishment.

Furthermore, treated Na-K alloy anode can derive a better plating/stripping stability compared with the untreated one. Tu [13] stated that Na-K with solid K_2O interface exhibits only 2/3 voltage polarization than untreated Na-K alloy, which is because the K_2O layer can provide better interfacial adhesion to anchor the Na-K alloy. Besides, its physical self-healing ability renders a recovery ability of voltage hysteresis after high-rate plating/stripping. This is to say, to some extent, the better the wettability is, the more stable the voltage hysteresis.

When matched with appropriate cathode materials, asymmetric batteries were set up to have a comprehensive electrochemical cognition of Na-K based full batteries with different wettability treatment strategies as listed in Table 1. Four strategies all contribute satisfactory and close electrochemical performance in specific capacity and retention rate. However, the electrochemical properties are influenced by a variety of variables such as electrolyte, cathode materials, wettability treatment. Therefore, electrochemical analysis requires experiments such as plating/striping on anode and intercalation/de-intercalation on cathode. Interestingly, researchers find the dominant ionic carrier will change during the electrochemical process, scilicet, the Na-K asymmetric batteries can flexibly be the potassium-ion batteries or the sodium-ion batteries. Hence, it is crucial to find out the key factors to determine the selectivity of the dominant ionic carrier.

4. Selection mechanism of dominant ionic carrier

Analyzing cathode products and voltage change during the charge–discharge process will clarify the specific dominant ionic carrier. This article classifies the key factors into the perspectives of intrinsic ionic property, initial electrolyte, cathode material, separator and SEI.

As for thermodynamics, K^+ possesses stronger reducibility than Na^+ in the same solvent, *i.e.*, the oxidation potential of K [−2.92 V *vs.* standard hydrogen electrode (SHE)] is lower than Na (−2.71 V *vs.* SHE). Hence, K is more likely to be oxidized into K^+, thus existing in the electrode as the dominant ionic carrier without considering the existing carriers in the initial electrolyte. However, Na^+ in the electrolyte can also become the dominant ionic carrier, *e.g.*, a Na-based electrolyte ($NaPF_6$, $NaClO_4$) will provide ample Na^+ during cycles. Thus, it is vital to make certain the conclusive factor in the selection of the dominant ionic carrier that is determined by the ion property or the ionic carrier existing in the initial electrolyte.

Kang [37] and Goodenough [22] have proven the ion property dominated mechanism, as shown in Fig. 3a. Kang prepared a metal–oxygen system with a Na-K alloy as the anode and assembled K-O_2 and Na-O_2 batteries in DEGDME solvent with KPF_6 salt and $NaPF_6$ salt.

Ascribed to the lower oxidation potential of K and the high concentration of K^+ in KPF_6 in DEGDME, the X-ray diffraction (XRD) patterns of the K-O_2 battery showed that the cathode products were KO_2 [55–57] and a small amount of KOH. This proved that K^+ was the dominant ionic carrier in this system, which resulted from the synergistic effect under thermodynamics and the initial electrolyte. It is noteworthy that in the Na-O_2 battery, the original Na^+ in $NaPF_6$ tended to dominate; however, the thermodynamic inclination caused by the ionic property still favored K^+ as the dominant ionic carrier. Hence, the effects of the ionic property and the initial electrolyte formed a comparative relationship. Kang revealed this contradiction. Based on the cathode characterization, the cycle products were a Na-based product (NaO_2) and K-based products (KO_2 and KOH), and the latter increased with increasing time. Fig. 3a demonstrates that the orange Na^+ ions initially take

Table 1
Features and electrochemical properties of four wettability treatment strategies.

Method	Pros	Cons	Electrochemical properties
High-temperature induction	①High spreadability	①Temperature at 420 °C; ②Thermal management cost	122 mAh/g at 1C matched by $MnFe(CN)_6^{2-}$; 97% retained at 400 cycles [22] ≈97% retained at 100 cycles
Capillary effect	①Room temperature ②Stable adsorption	①Require specific structure	85 mAh/g at 10C matched by $Na_3V_{2(}PO4)_3$; 85% retained at 1000 cycles [30] ≈97% retained at 100 cycles
Vacuum infiltration	①Uniform distribution ②Feasibility	①Require rigorous atmosphere	110 mAh/g at 1C matched by $K_2MnFe(CN)_6$; 86% retained at 100 cycles [31]
Solid interface protection	①Tension eliminated ②Self-healing ability	①Require pretreatment	103 mAh/g at 1A/g matched by PB; 91% retained at 150 cycles [13] ≈93% retained at 100 cycles

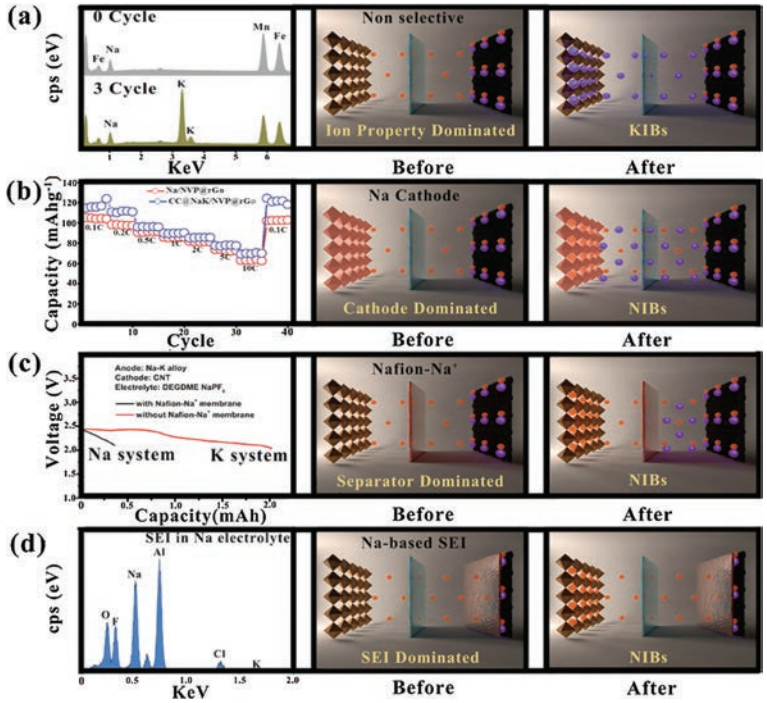

Fig. 3. Four ionic carrier selection mechanisms and evolution based on the initial Na^+ electrolyte, with orange balls referring to Na^+ and purple balls referring to K^+ in sandwich batteries. (a) Ion property dominated. Reproduced with permission [23]. Copyright 2018, Wiley. (b) Cathode dominated. Reproduced with permission [30]. Copyright 2020, Electrochemical Society, Inc. (c) Separator dominated. Reproduced with permission [38]. Copyright 2018, American Chemical Society. (d) SEI dominated. Reproduced with permission [33]. Copyright 2019, Wiley.

advantage of the high concentration in the electrolyte as the dominant ionic carrier of the Na-O_2 battery in the first few cycles. As the reaction continues, the metallic thermodynamics drive the increase of purple K^+ ions in Fig. 3a, causing K^+ to become the dominant ionic carrier. In other words, the Na-O_2 battery is replaced by the K-O_2 battery [58].

Likewise, Kang verified the role of separator in carrier selectivity by a compensation experiment. He adopted a Nafion-Na^+ separator as exhibited in Fig. 3c, where the red separator will only enable Na^+ to transmit. He observed a dramatic decrease in the overall capacity of the battery compared with the common separator, which is regarded as the result that K^+ cannot pass the Nafion-Na separator. This experiment proved that the separator is a direct determinant in carrier selectivity.

In accordance with Kang's conclusion, Goodenough observed a similar transformation in a metal battery [22] that supports K^+ as the determinant ion carrier in Na-K anodes. He adopted a Na-K alloy and carbon paper as the KNC anode, desodiated $Na_2MnFe(CN)_6$ as the cathode, and 1 mol/L $NaClO_4$ [10 wt% FEC] as the electrolyte to explore the influence of metallic intrinsic properties and the electrolyte on carrier selectivity. Analysis of cycle cathode products by energy-dispersive X-ray spectroscopy (EDS) revealed that the change in the proportion of Na^+ and K^+ after three cycles was more apparent than after the first cycle in which the K^+ products appeared; in addition, the peak intensity of the Na^+ products decreased gradually. After 65 cycles, the peak intensity of Na^+ disappeared completely and the EDS results no longer changed. The XRD results confirmed that the desodiated $Na_2MnFe(CN)_6$ transformed to $K_2MnFe(CN)_6$ after several cycles. The electrochemical characterization showed that the discharge voltage increased gradually during cycling indicating that K^+ was dominant in the electrolyte due to its ionic property. In this process, K^+ moved from the anode to the electrolyte and Na^+ moved from the electrolyte to the anode, facilitating the transformation of the $NaClO_4$ salt to $KClO_4$. Notably, the desodiated $Na_2MnFe(CN)_6$ accomplished simultaneous intercalation of K^+ and Na^+, which revealed that this cathode had no influence on the selectivity of carrier, and thus, it was not a variable in the experiment.

In summary, providing that the cathode material and the separator are not ionic selective mediums, as displayed in Fig. 3a, the advantage of the initial electrolyte can be overcome by the K^+ property of lower oxidation potential and eventually form a K^+-dominated carrier system.

The former experiments employed a nonselective cathode that accommodated both Na^+ and K^+; however, through further research, the carrier selectivity of cathode will determine the sustainability of the system shown in Fig. 3b. Therefore, $Na_3V_2(PO_4)_3$ [30], $Na_{2/3}Ni_{1/3}Mn_{2/3}O_2$ (NNMO), and $K_2MnFe(CN)_6$ (KMFC) [31] have been used as single ion cathodes in research. Zhang [30] adopted a Na-K alloy immersed in a porous nanocarbon cloth after high-temperature treatment to form a CC@NaK anode and $Na_3V_2(PO_4)_3$ covered by graphene oxide (C: 11.9 wt%) to form a NVP@rGo cathode. Because of the radius of the ion, $Na_3V_2(PO_4)_3$ prohibits the insertion of K^+, as shown by the orange cathode in Fig. 3b. After 100 cycles at 1C, K was absent in the EDS spectrum of the cathode, which proved that the role of the Na-K alloy was similar to that of the Na anode in this case. Goodenough [31] also achieved single selectivity of the carrier through NNMO and KMFC to construct full batteries with the same $NaClO_4$ electrolyte. In the NNMO system, the battery maintained a Na^+-dominated system and experienced 500 cycles at 1C, and the average Coulombic efficiency was 99.80%; in the KMFC system, the transformation of the electrolyte from $NaClO_4$ to $KClO_4$ based on the intrinsic property of K^+ was observed, and the average Coulombic efficiency after 100 cycles at 1C was 98.38%. This research revealed that the cathode can also influence the carrier selectivity, regardless of the ionic property.

Several studies have examined whether SEI also influences the selectivity of carriers. Yu [32] reported a set of comparative

Table 2
Wettability treatment and carrier selection in recent articles.

Cathode	Electrolyte	Wettability treatment	Carrier selection	Type	Reference
CNT	KPF_6 in DEGDME	Not reported	Ion property dominated	K type	[37]
Ditto	$NaPF_6$ in DEGDME	Not reported	Separator dominated	Na type	
NVP@rGo	$NaClO_4$ in PC	Capillary effect	Cathode dominated	Na type	[30]
(CNF)/SR	$NaClO_4$ in EC:DEC	Vacuum infiltration	SEI dominated	Na type	[32]
Ditto	KFSI in DME	Ditto	Ditto	Na type	
Prussian blue	KPF_6 in EC:DEC	Solid interface protection	Ion property dominated	K type	[33]
$MnFe(CN)_6^{2-}$	$NaClO_4$ in EC:DEC	High-temperature induction	Ion property dominated	K type	[22]
Activated Carbon	KPF_6 in DEGDME	Capillary effect	Ion property dominated	K type	[34]
Prussian blue	KPF_6 in EC:DEC	Solid interface protection	Ion property dominated	K type	[13]
$Na_{2/3}Ni_{1/3}Mn_{2/3}O_2$	$NaClO_4$ in PC	Vacuum infiltration	Cathode dominated	Na type	[31]
$K_2MnFe(CN)_6$	$KClO_4$ in PC	Ditto	Ditto	K type	

experiments in which KIB and SIB were prepared using KFSI (in DME) and $NaClO_4$ (in EC:DEC = 1:1, 10 wt% FEC) electrolytes and the nonselective organic cathode sodium rhodizonate dibasic (SR), respectively. XPS and EDS demonstrated that the SEI was mainly composed of KF, the decomposition product F–S, and carbonate (C = O, C-O) [59]. The structure of the SEI had two main layers: the porous organic surface enabled the transmission of both alkaline ions and anions; the compact inorganic subsurface exclusively enabled anions [60]. In this case, the SEI of the SIB mainly contained NaF, Na_2O, the decomposition product FEC, and carbonate [61,62], without a K compound. According to the voltage stability after 100 cycles and the EDS of the cathode products, Yu considered that the dominant carrier was not conserved during the process (especially in SIB). Based on the properties of SEI, such as inhibiting the transmission of electrons and permitting the diffusion of carriers exclusively [22,63], Yu speculated that in the SEI based on the Na-electrolyte in Fig. 3d, the orange SEI layer only allows Na^+ to pass through and inhibits K^+. More interestingly, this view did not conform to the observations by Kang [37] and Goodenough; they had also adopted an unselective cathode and $NaClO_4$ (FEC 10 wt%) as the electrolytes to construct an Na-based battery based on an Na-K anode. The battery finally transformed to a K-based battery. This contradiction was the result of the use of different solvents in the three studies. Kang adopted DEGME, Goodenough adopted PC mixed with FEC, and Yu adopted EC:DEC. Because of the better film-forming characteristics of EC:DEC than those of PC or DEGDME [64,65] and the different ingredients of salts, there were differences in the composition and structure of SEI, which led to different selective results. Further investigation is needed to understand the detailed mechanism for SEI selectivity.

In conclusion, as listed in Table 2, the concentration of the original carrier in an electrolyte dominates initially; however, the intrinsic property of K^+ will gradually dominate during further cycles. More importantly, the selection of the cathode, separator, and SEI will directly determine the dominant ionic carrier in the electrochemical and physical inhabitation of exclusionary ions.

5. Conclusion and perspectives

If the cathode, separator, and SEI do not confine K^+ specifically, regardless of the choice of electrolyte, the dominant ionic carrier in Na-K alloy batteries is K^+. Furthermore, the use of ether electrolyte can result in an unstable liquid–liquid interface, leading to low Coulombic efficiency and poor rate capability. Instead, Na-K alloys are compatible with many ester solutions, such as EC, PC, FEC, DEC, and DMC. In the selection of the electrolytes, the solubility of $KClO_4$ is relatively low; however, KPF_6, KFSI, KTFSI, and other new electrolytes or binders need more supporting experimental statistics to demonstrate their compatibility with the Na-K alloy interface.

In the application of the properties of liquid Na-K alloys, flexible devices such as soft pack batteries and flexible electronics are good choices in energy storage. Good ductility was discovered in a non-Newtonian Na-K coating adopting Al foil as the collector, silk stockings as the separator, and rubber gloves as a flexible substrate. It sustained more than 200% flexibility and $\pm 90^\circ$ reversal, with lasting charging and discharging. The high ductility enabled the device to adapt to the structure of humans and fit well into the human body, thus showing great superiority and potential in wearable devices compared with traditional rigid batteries. This liquid alloy anode also gave novel insight into the development of flow batteries, with promising properties in grid-scale batteries.

However, lots of issues remain to be solved in practice. Because of high chemical activity of the Na-K alloy, effective strategies in device design are necessary to avoid the introduction of impurities during alloy preparation, and contact with moisture and oxygen while using is a security risk as well.

In brief, more studies are needed to explore new solutions of surface tension, to seek new structures of the liquid–liquid interface, to establish comprehensive design involved current collector and electrolyte, to introduce self-healing with a non-dendrite-depositing intermediate phase, and to maximize the energy density of the dominant ionic carrier through the use of reasonable Na-K proportions. Although four ionic carrier selection mechanisms are presented qualitatively, more precise mechanisms need to be elucidated that combine experiments and material computation, especially in the selectivity of electrolytes and cathodes.

Declaration of competing interest

The authors report no declarations of interest.

Acknowledgments

This work was supported by National Defense Science and Technology Innovation Special Zone Projects (No. 18-163-21-TS-001-046-01), Sichuan Science and Technology Program (Nos. 20ZDYF0274, 20ZDYF0857, 2019ZDZX0002) and the Fundamental Research Funds for the Central Universities (No. ZYGX2019Z022).

Appendix A. Supplementary data

Supplementary material related to this article can be found, in the online version, at doi:https://doi.org/10.1016/j.cclet.2020.09.018.

References

[1] K. Yan, Z. Lu, H.W. Lee, et al., Nat. Energy 1 (2016) 16010.
[2] A. Pei, G. Zheng, F. Shi, Y. Li, Y. Cui, Nano Lett. 17 (2017) 1132–1139.
[3] J.N. Chazalviel, Phys. Rev. A 42 (1990) 7355–7367.

[4] V. Fleury, J.N. Chazalviel, M. Rosso, B. Sapoval, J. Electroanal. Chem. 290 (1990) 249–255.
[5] J. Lee, Y. Lee, J. Lee, et al., ACS Appl. Mater. Interfaces 9 (2017) 3723–3732.
[6] J. Zheng, S. Chen, W. Zhao, et al., ACS Energy Lett. 3 (2018) 315–321.
[7] Y. Zhao, L.V. Goncharova, Q. Zhang, et al., Nano Lett. 17 (2017) 5653–5659.
[8] Y. Zhao, L.V. Goncharova, A. Lushington, et al., Adv. Mater. 29 (2017) 1606663.
[9] W. Luo, C.F. Lin, O. Zhao, et al., Adv. Energy Mater. 7 (2017) 1601526.
[10] P. Zou, Y. Wang, S.-W. Chiang, et al., Nat. Commun. 9 (2018) 1–9.
[11] K. Chen, R. Pathak, A. Gurung, et al., Energy Stor. Mater. 18 (2019) 389–396.
[12] X. Chen, X.R. Chen, T.Z. Hou, et al., Sci. Adv. 5 (2019) eaau7728.
[13] L. Zhang, X. Xia, Y. Zhong, et al., Adv. Mater. 30 (2018) 1804011.
[14] H. Kim, D.A. Boysen, J.M. Newhouse, et al., Chem. Rev. 113 (2013) 2075–2099.
[15] X. Lu, G. Li, J.Y. Kim, et al., Nat. Commun. 5 (2014) 1–8.
[16] H. Li, H. Yin, K. Wang, et al., Adv. Energy Mater. 6 (2016) 1600483.
[17] J. Liu, J.G. Zhang, Z. Yang, et al., Adv. Funct. Mater. 23 (2013) 929–946.
[18] K.B. Hueso, M. Armand, T. Rojo, Energy Environ. Sci. 6 (2013) 734–749.
[19] D.J. Bradwell, H. Kim, A.H. Sirk, D.R. Sadoway, J. Am. Chem. Soc. 134 (2012) 1895–1897.
[20] K. Wang, K. Jiang, B. Chung, et al., Nature 514 (2014) 348–350.
[21] J.T. Kummer, W. Neill, Google Patents, 1968.
[22] L. Xue, H. Gao, W. Zhou, et al., Adv. Mater. 28 (2016) 9608–9612.
[23] H. Ye, C.Y. Wang, T.T. Zuo, et al., Nano Energy 48 (2018) 369–376.
[24] N. Xiao, W.D. McCulloch, Y. Wu, J. Am. Chem. Soc. 139 (2017) 9475–9478.
[25] E. Shpil'rain, V. Savchenko, A.G. Mozgovoi, S.N. Skovorod'ko, High Temp. 41 (2003) 23–31.
[26] A.G. Mozgovoi, V.V. Roshchupkin, S.N. Skovorod'ko, M.A. Pokrasin, A.I. Chernov, High Temp. 41 (2003) 340–345.
[27] K. Khoshmanesh, S.Y. Tang, J.Y. Zhu, et al., Lab Chip 17 (2017) 974–993.
[28] A. Zavabeti, J.Z. Ou, B.J. Carey, et al., Sci. Adv. 358 (2017) 332–335.
[29] Y. Jin, K. Liu, J. Lang, et al., Nat. Energy 3 (2018) 732–738.
[30] Y. Xie, J. Hu, Z.J. Zhang, J. Electroanal. Chem. 856 (2020) 113676.
[31] L. Xue, W. Zhou, S. Xin, et al., Angew. Chem. Int. Ed. 130 (2018) 14380–14383.
[32] Y. Ding, X. Guo, Y. Qian, et al., Adv. Mater. 31 (2019) 1806956.
[33] L. Zhang, Y. Li, S. Zhang, et al., Small Methods 3 (2019) 1900383.
[34] L. Qin, W. Yang, W. Lv, et al., Chem. Commun. 54 (2018) 8032–8035.
[35] Z. Xu, M. Wu, Z. Chen, et al., Adv. Sci. 6 (2019) 1802272.
[36] Z. Chen, W. Li, J. Yang, et al., J. Electrochem. Soc. 167 (2020) 050506.
[37] W. Yu, K.C. Lau, Y. Lei, et al., ACS Appl. Mater. Interfaces 9 (2017) 31871–31878.
[38] A.C. Baclig, G. McConohy, A. Poletayev, et al., Joule 2 (2018) 1287–1296.
[39] Y. Zhao, X. Yang, L.Y. Kuo, et al., Small Methods 14 (2018) 1703717.
[40] D. Lin, Y. Liu, Z. Liang, et al., Nat. Nanotechnol. 11 (2016) 626–632.
[41] G. Sahu, Z. Lin, J. Li, et al., Energy Environ. Sci. 7 (2014) 1053–1058.
[42] L. Porcarelli, C. Gerbaldi, F. Bella, J. Nair, Sci. Rep. (2016) 19892.
[43] L. Zhang, S. Peng, Y. Ding, et al., Energy Environ. Sci. 12 (2019) 1989–1998.
[44] Z. Xu, J. Chen, M. Wu, et al., Electron. Mater. Lett. 15 (2019) 428–436.
[45] J.L. Dye, K.D. Cram, S.A. Urbin, et al., J. Am. Chem. Soc. 127 (2005) 9338–9339.
[46] J.L. Dye, P. Nandi, J.E. Jackson, et al., Chem. Mater. 23 (2011) 2388–2397.
[47] W. Go, M.-H. Kim, J. Park, et al., Nano Lett. 19 (2018) 1504–1511.
[48] S. Wang, J. Liao, M. Wu, et al., Part. Part. Syst. Charact. 34 (2017) 1700141.
[49] J. Desreumaux, M. Calais, R. Adriano, et al., Eur. J. Inorg. Chem. 2000 (2000) 2031–2045.
[50] Nguefack, Eur. J. Inorg. Chem. (2000) 2031–2045.
[51] Y. Ding, X. Guo, Y. Qian, et al., Adv. Mater. 32 (2020) 2002577.
[52] L. D, H. YB, H. H, et al., Z. S. Nat. Commun. 10 (2019) 4244.
[53] P. Liu, Y. Wang, Q. Gu, et al., Adv. Mater. 32 (2020) 1906735.
[54] X. Lin, Q. Sun, K.D. Davis, R. Li, X. Sun, Carbon Energy 1 (2019) 141–164.
[55] X. Ren, Y. Wu, J. Am. Chem. Soc. 135 (2013) 2923–2926.
[56] C.O. Laoire, S. Mukerjee, K. Abraham, E.J. Plichta, M.A. Hendrickson, J. Phys. Chem. C 113 (2009) 20127–20134.
[57] C. Bondue, P. Reinsberg, A. Abd-El-Latif, H. Baltruschat, Phys. Chem. Chem. Phys. 17 (2015) 25593–25606.
[58] L. Xue, Y. Li, H. Gao, et al., J. Am. Chem. Soc. 139 (2017) 2164–2167.
[59] N. Xiao, W.D. McCulloch, Y.J. Wu, Energy Stor. Mater. 139 (2017) 9475–9478.
[60] C.Z. Zhao, X.B. Cheng, R. Zhang, et al., Energy Stor. Mater. 3 (2016) 77–84.
[61] L. Ji, M. Gu, Y. Shao, et al., Adv. Mater. 26 (2014) 2901–2908.
[62] P. Baglioni, J. Solution Chem. 44 (2015) 1224–1239.
[63] Z.W. Seh, J. Sun, Y. Sun, Y. Cui, ACS Cent. Sci. 1 (2015) 449–455.
[64] G.G. Eshetu, S. Grugeon, H. Kim, et al., ChemSusChem 9 (2016) 462–471.
[65] H. Che, S. Chen, Y. Xie, et al., Energy Environ. Sci. 10 (2017) 1075–1101.